Volume 12
Number 22
21 November 2025
Pages 9321–9854

Materials Horizons

rsc.li/materials-horizons

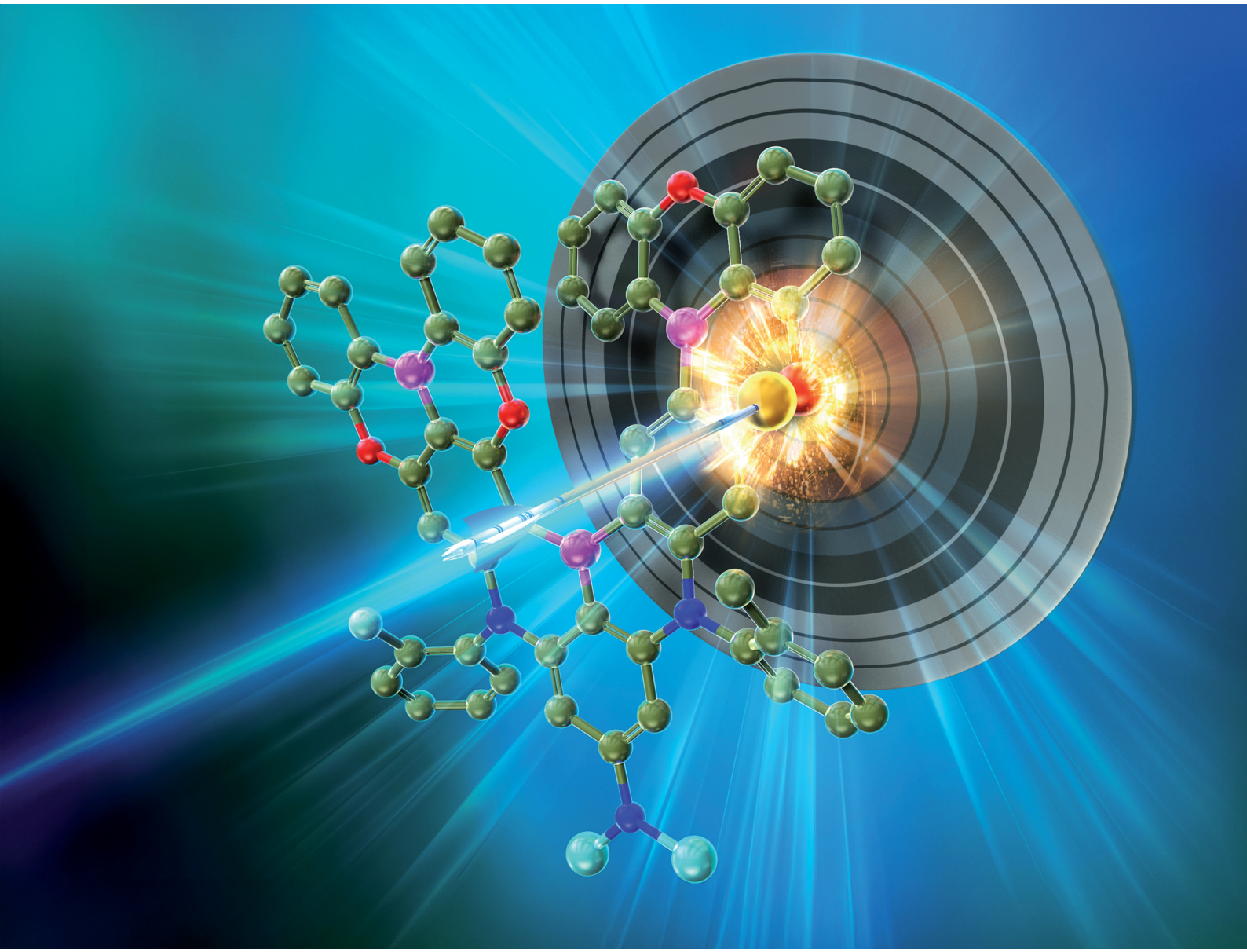

ISSN 2051-6347

ROYAL SOCIETY OF CHEMISTRY

COMMUNICATION

Takuji Hatakeyama *et al.*

Improving the TADF properties of deep-blue multiple-resonance emitters by strategic oxygen–sulfur replacement

Materials Horizons

ROYAL SOCIETY OF CHEMISTRY

COMMUNICATION

View Article Online
View Journal | View Issue

Check for updates

Cite this: *Mater. Horiz.*, 2025, **12**, 9556

Received 16th July 2025,
Accepted 23rd September 2025

DOI: 10.1039/d5mh01353d

rsc.li/materials-horizons

Published on 08 October 2025. Downloaded on 3/14/2026 9:21:18 PM.

Improving the TADF properties of deep-blue multiple-resonance emitters by strategic oxygen–sulfur replacement

Junki Ochi,[a] Yuki Yamasaki,[b] Susumu Oda,[c] Masakazu Kondo,[d] Yasuhiro Kondo,[e] Masahiro Hayakawa[a] and Takuji Hatakeyama[*a]

An oxygen–sulfur replacement for improving thermally activated delayed fluorescence (TADF) materials based on a multiple-resonance (MR) effect is reported. A comprehensive computational analysis of four possible isomers revealed that the precise placement of the sulfur atom is crucial to suppress undesired spectral red-shifts. Among them, a promising deep-blue emitter, DOB2-DABNA-C-NP-S-1, exhibits emission at 458 nm with a narrow full width at half maximum (FWHM) of 20 nm. Moreover, its reverse intersystem crossing rate constant (k_{RISC}) of 2.9 × 10^6 s^{-1} is three times larger than that of the oxygen-based analog (9.0 × 10^5 s^{-1}). An OLED device incorporating DOB2-DABNA-C-NP-S-1 as an emitter achieves ultrapure deep-blue electroluminescence at 461 nm with Commission Internationale de l'Éclairage (CIE) coordinates of (0.133, 0.077), satisfying the blue emitter standards set by the National Television System Committee (NTSC). The device demonstrates outstanding external quantum efficiencies (EQEs) of 24.3% (at maximum), 23.9% (at 1000 cd m^{-2}), and 18.7% (at 10 000 cd m^{-2}), with the latter ranking the highest among the previously reported OLED devices employing deep-blue MR-TADF emitters.

New concepts

Introducing heavy atoms into the MR-TADF framework is one of the most common approaches to improve TADF performance. However, replacing oxygen with sulfur often causes a red-shift in photoluminescence, especially in deep-blue emitters, thereby compromising the color purity of the original oxygen-containing compounds. To address this issue, we demonstrate that regulating the LUMO energy level is key to maintaining deep-blue even after sulfur incorporation. A comprehensive analysis of four sulfur-containing isomers revealed that the careful selection of the oxygen–sulfur substitution site can effectively suppress the undesired spectral red-shift. Based on these insights, we synthesized **DOB2-DABNA-C-NP-S-1** as a sulfur-incorporated MR-TADF emitter. The OLED device employing this compound exhibited deep-blue electroluminescence (461 nm) with suppressed efficiency roll-off (external quantum efficiency (EQE) = 24.3%/23.9%/18.7% at maximum/1000/10 000 cd m^{-2}) and a device lifetime (LT50) of 39 h at 500 cd m^{-2}. Notably, an EQE of 18.7% at 10 000 cd m^{-2} ranks among the highest reported for the deep-blue OLED using MR-TADF materials. These results demonstrate a general molecular design strategy for achieving deep-blue emission in heavy-atom incorporating MR-TADF materials, which has remained largely unexplored to date.

Introduction

Thermally activated delayed fluorescence (TADF) materials[1,2] have garnered significant attention in the field of organic light-emitting diodes (OLEDs)[3] due to their capability to utilize all excitons generated by electric field excitation. To enable highly efficient and color-pure TADF emission for advanced OLED technology, our group introduced a novel design principle in 2016, namely the multiple resonance (MR) effect.[4] This approach provides a powerful solution for simultaneously achieving both high photoluminescence quantum yield (PLQY) and narrow full width at half maximum (FWHM). These attractive features originate from the unique electronic structure created by alternating electron-donating and electron-accepting atoms attached to a single benzene ring. This specific arrangement induces contrasting resonant features, effectively localizing the highest occupied molecular orbital (HOMO) and lowest unoccupied molecular orbital (LUMO) onto distinct carbon atoms. Consequently, MR-TADF emitters exhibit highly desirable narrow-band emission, enabling the realization of superior color purity in OLEDs without the need for energy-consuming color filtering.[5,6]

To improve the device performance of OLEDs fabricated with MR-TADF emitters, their reverse intersystem crossing

[a] *Department of Chemistry, Graduate School of Science, Kyoto University, Sakyo-ku, Kyoto 606-8502, Japan. E-mail: hatake@kuchem.kyoto-u.ac.jp*
[b] *Department of Chemistry, Graduate School of Science and Technology, Kwansei Gakuin University, 2-1 Gakuen, Sanda, Hyogo 669-1337, Japan*
[c] *Department of Applied Chemistry, Graduate School of Science and Engineering, Toyo University, 2100 Kujirai, Kawagoe, Saitama 350-8585, Japan*
[d] *JNC Co., Ltd., 5-1 Goikaigan, Ichihara, Chiba 290-8551, Japan*
[e] *SK JNC Japan Co., Ltd., 5-1 Goikaigan, Ichihara, Chiba 290-8551, Japan*

This journal is © The Royal Society of Chemistry 2025

Published on 08 October 2025. Downloaded on 3/14/2026 9:21:18 PM.

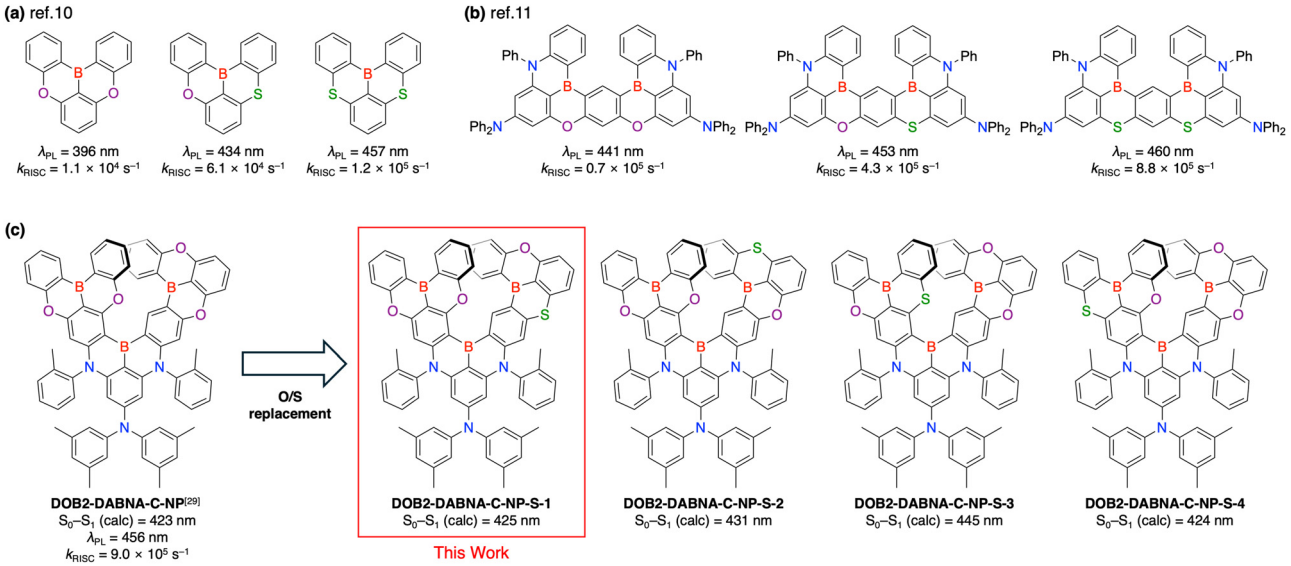

Fig. 1 (a) and (b) Previous examples of oxygen–sulfur replacement.[10,11] (c) Molecular structure of four O3S-type isomers and their predicted excitation wavelength of the S_0–S_1 transition calculated at the B3LYP/6-31G(d) level of theory.

(RISC) rate constant (k_{RISC}) is a significant parameter because accumulated triplet excitons can lead to quenching processes such as triplet–triplet annihilation (TTA) and triplet–polaron annihilation (TPA). One of the most common strategies to enhance k_{RISC} is introducing heavy atoms into the MR framework.[7–9] For example, Shao, Wang, and coworkers first performed a direct comparison of oxygen- and sulfur-attached MR-TADF emitters and revealed the enhanced spin–orbit coupling (SOC) matrix element and accelerated RISC (Fig. 1a).[10] Similarly, Park, Yasuda, and coworkers reported deep-blue MR-TADF emitters embedding sulfur atoms, whose k_{RISC} was up to 12 times higher than that of the oxygen-bridged analog (Fig. 1b).[11] Although the heavy-atom effect of sulfur (Z_N = 16) is considered to be not so significant, these results clearly prove the validity of oxygen–sulfur replacement. Stimulated by these pioneering works, many research studies have been conducted from both synthetic[12–25] and computational[26–28] approaches, attempting to improve the TADF properties of MR-emitters. However, the incorporation of sulfur atoms often causes a red-shift in photoluminescence, especially in deep-blue emitters, thereby compromising the color purity of the original O-containing compounds (Table S7). For precise and strategic design of high-performance MR-TADF emitters, deeper understanding of the effect of oxygen–sulfur replacement is necessary.

With these circumstances in mind, herein, we focus on the improvement of **DOB2-DABNA-C-NP**, a π-extended MR-TADF material reported by our group (Fig. 1c).[29] This compound, which contains four oxygen atoms, exhibits deep-blue fluorescence (456–458 nm) and a fast k_{RISC} (0.8–1.1 × 10^6 s^{-1}), leading to a remarkable OLED performance with an external quantum efficiency (EQE) of 20.8% at 1000 cd m^{-2}. After a comprehensive computational analysis of all four candidates generated by oxygen–sulfur replacement of **DOB2-DABNA-C-NP**, we expect **DOB2-DABNA-C-NP-S-1** to be a promising candidate for an improved deep-blue MR-TADF emitter. Motivated by this prediction, **DOB2-DABNA-C-NP-S-1** was synthesized, and its photophysical properties were investigated, revealing an improved k_{RISC} (2.9 × 10^6 s^{-1}) while maintaining pure blue emission (458 nm). The OLED device fabricated with **DOB2-DABNA-C-NP-S-1** exhibited Commission Internationale d'Éclairage (CIE) coordinates of (0.133, 0.077), which satisfy the blue gamut standard defined by the National Television System Committee (NTSC). Importantly, the efficiency roll-off is highly suppressed (EQE_{max} = 24.3%/EQE_{1000} = 23.9%) because of the improved k_{RISC} value, indicating the validity of precisely selecting the sulfur incorporation position.

Results and discussion

Molecular design

Fig. 2 shows the molecular orbitals of **DOB2-DABNA-C-NP** and its sulfur-incorporated analogs. Because the transition from HOMO−1 to LUMO is a main component of the S_0–S_1 excitation in all cases (Table S2), these two molecular orbitals are discussed here. First, regarding the HOMO−1 energy level, only small differences were observed among all compounds. This can be attributed to a faint contribution of oxygen and sulfur atoms to HOMO−1. On the other hand, the LUMO energy is largely perturbed by the oxygen–sulfur replacement. Moreover, the extent of this perturbation strongly depends on the sulfur position. In **DOB2-DABNA-C-NP-S-1** and **DOB2-DABNA-C-NP-S-4**, their LUMO energy was slightly stabilized from **DOB2-DABNA-C-NP** (0.021 eV). Much larger stabilization was observed in **DOB2-DABNA-C-NP-S-2** (0.061 eV) and **DOB2-DABNA-C-NP-S-3** (0.149 eV), which caused a red-shift characteristic of these two isomers (Fig. 1c). Such a sulfur-position dependency can be

Published on 08 October 2025. Downloaded on 3/14/2026 9:21:18 PM.

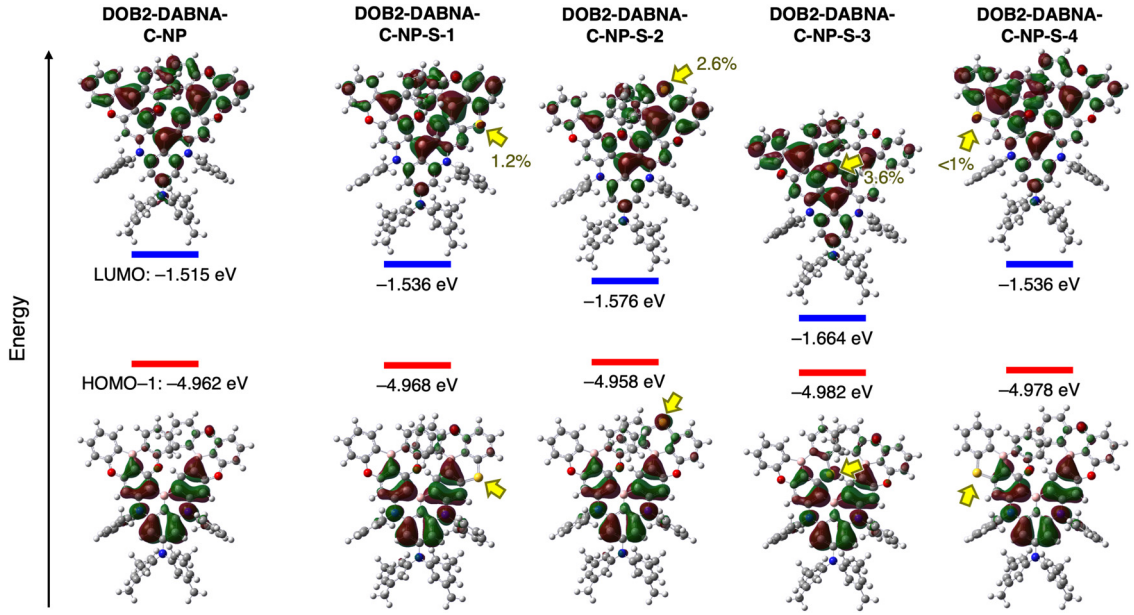

Fig. 2 HOMO−1 and LUMO of **DOB2-DABNA-C-NP** and its sulfur-incorporated analogs. Yellow arrows show the position of the incorporated sulfur atom.

rationalized by considering the anti-bonding character of two C–S bonds. While only one carbon atom adjacent to a sulfur atom shows a significant contribution to the LUMO in **DOB2-DABNA-C-NP-S-1** and **DOB2-DABNA-C-NP-S-4**, clear nodes can be observed in both C–S bonds in **DOB2-DABNA-C-NP-S-2** and **DOB2-DABNA-C-NP-S-3**, suggesting their contribution to the LUMO as an anti-bonding component. In these two isomers, therefore, the replacement by sulfur strongly shifts the LUMO energy through the perturbation of an anti-bonding character. In other words, the position where sulfur is incorporated in **DOB2-DABNA-C-NP-S-1** and **DOB2-DABNA-C-NP-S-4** does not largely participate in the LUMO, resulting in a small effect of the oxygen–sulfur replacement. These considerations are further supported by the population analysis, which proved that the contribution of a sulfur atom to the LUMO is larger in **DOB2-DABNA-C-NP-S-2** (2.6%) and **DOB2-DABNA-C-NP-S-3** (3.6%), thereby stabilizing their LUMO levels. Based on these results, we determined **DOB2-DABNA-C-NP-S-1** to be a target molecule to achieve deep-blue emission and an improved OLED device performance.

Synthesis

The synthetic scheme of **DOB2-DABNA-C-NP-S-1** is summarized in Fig. 3. The procedure is exactly the same as that for **DOB2-DABNA-C-NP**.[29] Starting from the previously reported compound **1**, the sulfur-containing unit **2**, which was synthesized in four steps from the commercially available materials, was introduced *via* Buchwald–Hartwig amination to afford **3** in 41% yield. After that, **DOB2-DABNA-C-NP-S-1** was synthesized by one-shot borylation[30–32] in 55% yield. Along with **DOB2-DABNA-C-NP**, the introduction of steric methyl groups in an appropriate position allowed a moderate yield of the final borylation reaction.

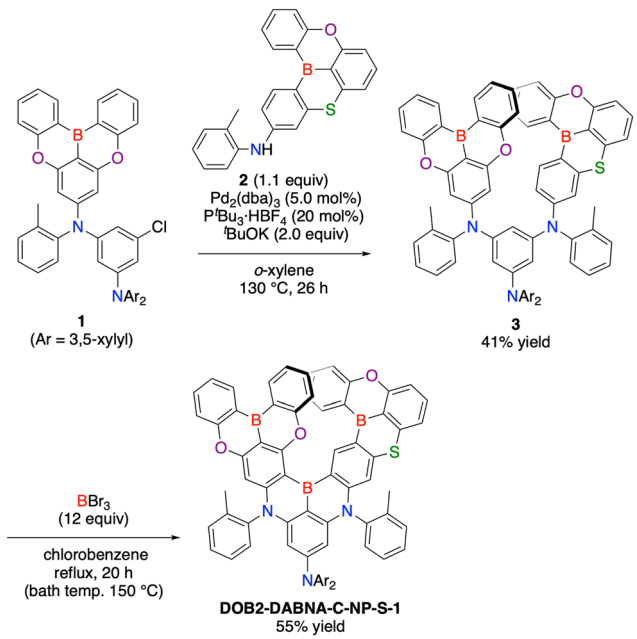

Fig. 3 Synthesis of **DOB2-DABNA-C-NP-S-1**.

Photophysical properties

Next, the photophysical properties of **DOB2-DABNA-C-NP-S-1** and **DOB2-DABNA-C-NP** were investigated under various conditions. To assess the impact of oxygen–sulfur replacement, toluene, poly(methyl methacrylate) (PMMA), and polystyrene (PS) were selected as matrices to mitigate specific intermolecular interactions with the surrounding molecules (Table S6). Fig. 4 summarizes the representative photophysical properties

 This journal is © The Royal Society of Chemistry 2025

Published on 08 October 2025. Downloaded on 3/14/2026 9:21:18 PM.

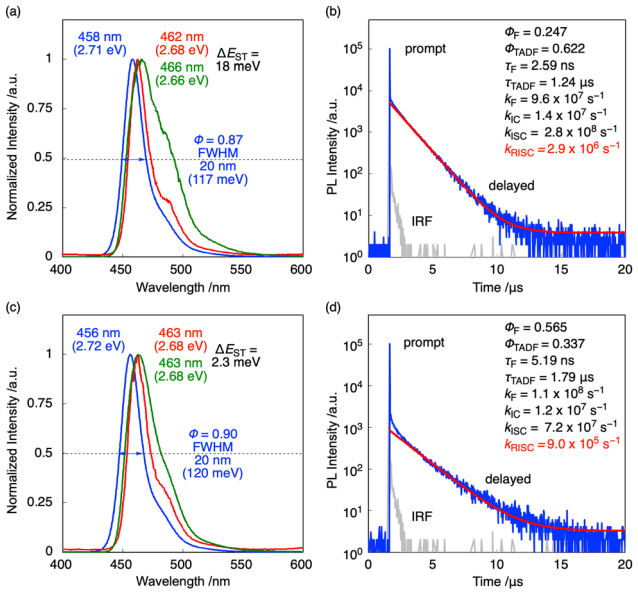

Fig. 4 Photophysical properties of (a) and (b) **DOB2-DABNA-C-NP-S-1** and (c) and (d) **DOB2-DABNA-C-NP** in PS 1 wt%-doped film. (a) and (c) Fluorescence spectra at 300 K (blue) and 77 K with (green) and without (red) a delay time of 25 ms. (b) and (d) Transient photoluminescence decay curve at 300 K and the relevant parameters. The red curve represents the single exponential fitting data (background = 3–4), and the gray curve represents an IRF curve.

measured in a 1 wt% emitter-doped PS film. As expected by the DFT calculation, **DOB2-DABNA-C-NP-S-1** exhibited a fluorescence maximum of 458 nm, which is only 2 nm red-shifted from **DOB2-DABNA-C-NP** (456 nm). The FWHM and the energy difference between the S_1 and T_1 states (ΔE_{ST}) were 20 nm (117 meV) and 18 meV, respectively. These values are also comparable to those of **DOB2-DABNA-C-NP**, confirming little loss of its attractive deep-blue character. Nevertheless, the rate constant of reverse intersystem crossing (k_{RISC}) of **DOB2-DABNA-C-NP-S-1** (2.9×10^6 s^{-1}) was 3.2 times larger than that of **DOB2-DABNA-C-NP** (9.0×10^5 s^{-1}). Thus, the oxygen–sulfur replacement effectively enhanced the TADF properties. Measurements in toluene and PMMA exhibited consistency with those in PS (Fig. S4 and S5). In addition, **DOB2-DABNA-C-NP-S-1** showed accelerated k_{RISC} and larger ΔE_{ST} compared to **DOB2-DABNA-C-NP** under all conditions. Given that the increased ΔE_{ST} is disadvantageous to the RISC process, the spin–orbit coupling (SOC) matrix should be enhanced by the oxygen–sulfur replacement. Although our computational SOC values largely depended on the conformation of the diphenylamine group, the higher k_{RISC} in **DOB2-DABNA-C-NP-S-1** could be reproduced by the semi-classical Marcus equation (Fig. S1 and Table S3).[33] Although intramolecular π–π interaction was observed by noncovalent interaction (NCI) analysis (Fig. S3),[34] the inclusion of Grimme's dispersion correlation parameters had a negligible effect on predicting the excited state properties (Tables S4 and S5). It should be noted that effects such as the

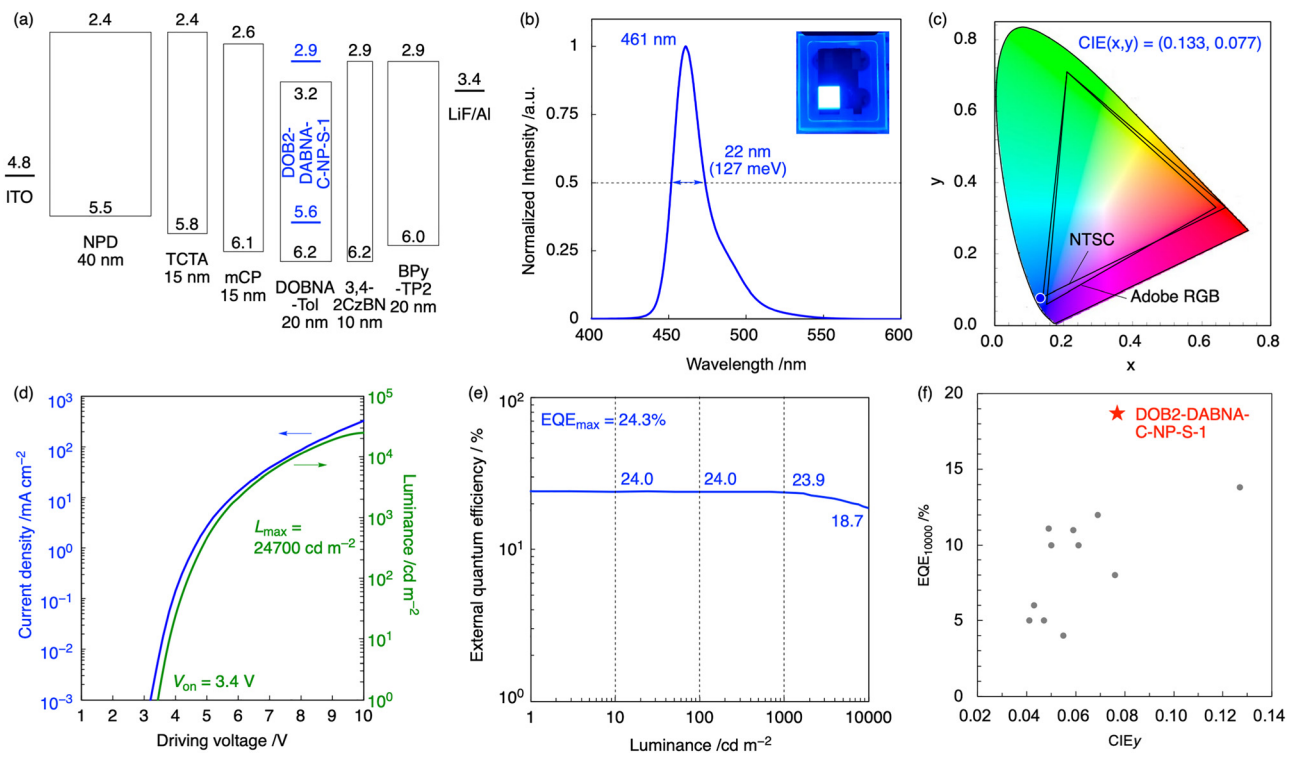

Fig. 5 OLED characteristics for the devices using **DOB2-DABNA-C-NP-S-1**. (a) Device structures with the estimated energy levels in eV for each component. (b) Normalized EL spectra. Inset: Electroluminescence of the device. (c) Commission Internationale de l'Éclairage (CIE) (*x*,*y*) coordinates. (d) Current density–voltage (*J*–*V*) characteristics (blue) and luminance–voltage (*L*–*V*) characteristics (green). (e) EQE–luminance (EQE–*L*) characteristics. (f) Comparison of EQE values at 10 000 cd m^{-2} with reported blue OLEDs.

Published on 08 October 2025. Downloaded on 3/14/2026 9:21:18 PM.

Herzberg–Teller vibronic coupling should be included for a more accurate SOC calculation.[35] These results prove that a careful choice of the replacement position successfully suppresses the red-shift in fluorescence and contributes to realizing improved deep-blue emission.

Electroluminescence properties

To evaluate the impact of the oxygen–sulfur replacement on OLED performance, a device using **DOB2-DABNA-C-NP-S-1** as an emitter was fabricated with the following structure: indium tin oxide (ITO, 50 nm); *N*,*N*′-di(1-naphthyl)-*N*,*N*′-diphenyl-(1,1′-biphenyl)-4,4′-diamine (NPD, 40 nm); tris(4-carbazolyl-9-ylphenyl)amine (TCTA, 15 nm); 1,3-bis(*N*-carbazolyl)benzene (mCP, 15 nm); 1 wt% **DOB2-DABNA-C-NP-S-1** emitter and 99 wt% **DOBNA-Tol**[36] (20 nm); 3,4-di(9*H*-carbazol-9-yl)benzonitrile (3,4-2CzBN,[37] 10 nm); 2,7-bis(2,2′-bipyridine-5-yl)triphenylene (BPy-TP2,[38] 20 nm); LiF (1 nm); and Al (100 nm) (Fig. 5a). The **DOB2-DABNA-C-NP-S-1**-fabricated device exhibited an ultrapure and narrow deep-blue emission (λ_{EL} = 461 nm, FWHM = 22 nm) (Fig. 5b). Its CIE coordinates were (0.133, 0.077), which are extremely close to the blue gamut standard defined by NTSC (CIE(x, y) = (0.14, 0.08)) (Fig. 5c). This device had a turn-on voltage of 3.4 V, showing typical semiconducting properties (Fig. 5d). While maintaining the desirable properties originally observed in the **DOB2-DABNA-C-NP**-fabricated device, the device performances, including EQE, current efficiency, power efficiency, and device lifetime, were improved by sulfur incorporation. The EQEs of the **DOB2-DABNA-C-NP-S-1**-based device reached 24.3/24.0/23.9% at the maximum, 100, and 1000 cd m^{-2}, respectively (Fig. 5e). These values were improved from the 21.7/21.4/20.8% observed in the **DOB2-DABNA-C-NP**-based device. Notably, the efficiency roll-off at 1000 cd m^{-2} was only 1.6%, an outstanding value compared to previous MR-emitter-based deep-blue OLED devices without a sensitizer (Table S8). The current and power efficiencies of the **DOB2-DABNA-C-NP-S-1**-based device at the maximum, 100, and 1000 cd m^{-2} were 17.3/16.9/16.9 cd A^{-1} and 16.9/12.1/9.8 lm W^{-1}, respectively (Fig. S13). These values also surpass those of the **DOB2-DABNA-C-NP**-based one (14.3/14.1/13.7 cd A^{-1} and 13.5/9.8/7.5 lm W^{-1}). The half-lifetime (LT_{50}) with an initial luminance of 500 cd m^{-2} was 39 h, which is 3.3 times longer than that of the previously reported **DOB2-DABNA-C-NP** device (Fig. S11). Notably, EQE_{10000} (18.7%) ranks the highest among the previously reported OLED devices employing deep-blue MR-TADF emitters (Fig. 5f and Table S9). Overall, the fast k_{RISC} of **DOB2-DABNA-C-NP-S-1**, benefiting from the oxygen–sulfur replacement, contributed to improved OLED performances while maintaining pure deep-blue electroluminescence.

Conclusions

In this study, we present a molecular design strategy for enhancing the performance of MR-TADF emitters through targeted oxygen–sulfur replacement. Rather than simple replacement, we systematically evaluated four regioisomeric sulfur analogues to determine how the substitution position influences the emission properties. Our analysis revealed that maintaining high excitation energy requires precise control over the LUMO level, which in turn depends critically on the sulfur atom's location. Among the candidates, **DOB2-DABNA-C-NP-S-1** emerged as a standout compound, exhibiting deep-blue photoluminescence at 458 nm with a narrow FWHM of 20 nm. These values are comparable to those of its oxygen-based counterpart, **DOB2-DABNA-C-NP**, thereby maintaining its desirable deep-blue character. Notably, the sulfur incorporation led to a threefold increase in the k_{RISC} compared to the oxygen-based emitter. The resulting OLED device delivered ultrapure deep-blue electroluminescence at 461 nm with CIE coordinates of (0.133, 0.077) and demonstrated excellent EQEs of 24.3%, 23.9%, and 18.7% at the maximum, 1000, and 10 000 cd m^{-2}, respectively. Notably, the $EQE_{10\,000}$ value surpasses that of all the previous OLED devices employing deep-blue MR-TADF emitters. These findings emphasize the importance of site-selective oxygen–sulfur replacement and offer valuable guidelines for the development of next-generation blue-emitting MR-TADF materials containing heavy atoms.

Conflicts of interest

There are no conflicts to declare.

Data availability

The data supporting this article have been included as part of the supplementary information (SI). Supplementary information is available. See DOI: **https://doi.org/10.1039/d5mh01353d**.

Acknowledgements

T. H. acknowledges Japan Science and Technology Agency (JST) CREST (grant no. JPMJCR22B3), the Japan Society for the Promotion of Science (JSPS) Fund for the Core-to-Core Program Number (grant no. JPJSCCA20220004), the Promotion of Joint International Research (ILR) (grant no. 23K20039), and Grants-in-Aid for Scientific Research (grant no. 24K01569). J. O. acknowledges the JSPS Fund for the Grant-in-Aid for Research Activity Start-up (grant no. 23K19245).

Notes and references

1 H. Uoyama, K. Goushi, K. Shizu, H. Nomura and C. Adachi, *Nature*, 2012, **492**, 234.
2 J. M. Dos Santos, D. Hall, B. Basumatary, M. Bryden, D. Chen, P. Choudhary, T. Comerford, E. Crovini, A. Danos, J. De, S. Diesing, M. Fatahi, M. Griffin, A. K. Gupta, H. Hafeez, L. Hämmerling, E. Hanover, J. Haug, T. Heil, D. Karthik, S. Kumar, O. Lee, H. Li, F. Lucas, C. F. R. Mackenzie, A. Mariko, T. Matulaitis, F. Millward, Y. Olivier, Q. Qi, I. D. W. Samuel, N. Sharma, C. Si, L. Spierling, P. Sudhakar, D. Sun, E. Tankelevičiūtė, M. Duarte Tonet, J. Wang, T. Wang, S. Wu,

 This journal is © The Royal Society of Chemistry 2025

Published on 08 October 2025. Downloaded on 3/14/2026 9:21:18 PM.

Y. Xu, L. Zhang and E. Zysman-Colman, *Chem. Rev.*, 2024, **124**, 13736.
3 C. W. Tang and S. A. VanSlyke, *Appl. Phys. Lett.*, 1987, **51**, 913.
4 T. Hatakeyama, K. Shiren, K. Nakajima, S. Nomura, S. Nakatsuka, K. Kinoshita, J. Ni, Y. Ono and T. Ikuta, *Adv. Mater.*, 2016, **28**, 2777.
5 M. Mamada, M. Hayakawa, J. Ochi and T. Hatakeyama, *Chem. Soc. Rev.*, 2024, **53**, 1624.
6 X. Wu, S. Ni, C.-H. Wang, W. Zhu and P.-T. Chou, *Chem. Rev.*, 2025, **125**, 6685.
7 H. J. Kim and T. Yasuda, *Adv. Opt. Mater.*, 2022, **10**, 2201714.
8 K. R. Naveen, P. Palanisamy, M. Y. Chae and J. H. Kwon, *Chem. Commun.*, 2023, **59**, 3685.
9 X.-F. Luo, X. Xiao and Y.-X. Zheng, *Chem. Commun.*, 2024, **60**, 1089.
10 F. Chen, L. Zhao, X. Wang, Q. Yang, W. Li, H. Tian, S. Shao, L. Wang, X. Jing and F. Wang, *Sci. China: Chem.*, 2021, **64**, 547.
11 I. S. Park, M. Yang, H. Shibata, N. Amanokura and T. Yasuda, *Adv. Mater.*, 2022, **34**, 2107951.
12 T. Hua, L. Zhan, N. Li, Z. Huang, X. Cao, Z. Xiao, S. Gong, C. Zhou, C. Zhong and C. Yang, *Chem. Eng. J.*, 2021, **426**, 131169.
13 Y. X. Hu, J. Miao, T. Hua, Z. Huang, Y. Qi, Y. Zou, Y. Qiu, H. Xia, H. Liu, X. Cao and C. Yang, *Nat. Photonics*, 2022, **16**, 803.
14 I. S. Park, H. Min and T. Yasuda, *Angew. Chem., Int. Ed.*, 2022, **61**, e202205684.
15 X.-F. Luo, H.-X. Ni, A.-Q. Lv, X.-K. Yang, H.-L. Ma and Y.-X. Zheng, *Adv. Opt. Mater.*, 2022, **10**, 2200504.
16 H. Gao, S. Shen, Y. Qin, G. Liu, T. Gao, X. Dong, Z. Pang, X. Xie, P. Wang and Y. Wang, *J. Phys. Chem. Lett.*, 2022, **13**, 7561.
17 H. Gao, Z. Li, Z. Pang, Y. Qin, G. Liu, T. Gao, X. Dong, S. Shen, X. Xie, P. Wang, C.-S. Lee and Y. Wang, *ACS Appl. Mater. Interfaces*, 2023, **15**, 5529.
18 X. Xiong, Y.-C. Cheng, K. Wang, J. Yu and X.-H. Zhang, *Mater. Chem. Front.*, 2023, **7**, 929.
19 M. Wang, Z. Fu, R. Cheng, J. Du, T. Wu, Z. Bin, D. Wu, Y. Yang and J. Lan, *Chem. Commun.*, 2023, **59**, 5126.
20 Z. Ye, H. Wu, Y. Xu, T. Hua, G. Chen, Z. Chen, X. Yin, M. Huang, K. Xu, X. Song, Z. Huang, X. Lv, J. Miao, X. Cao and C. Yang, *Adv. Mater.*, 2024, **36**, 2308314.
21 H.-X. Ni, J.-Z. Zhu, J.-J. Hu, L. Yuan, X.-J. Liao, S. Xing and Y.-X. Zheng, *Adv. Opt. Mater.*, 2024, **12**, 2401033.
22 L. Yuan, J.-W. Xu, Z.-P. Yan, Y.-F. Yang, D. Mao, J.-J. Hu, H.-X. Ni, C.-H. Li, J.-L. Zuo and Y.-X. Zheng, *Angew. Chem., Int. Ed.*, 2024, **63**, e202407277.
23 L. Yuan, Y.-F. Yang, Z.-P. Yan, J.-J. Hu, D. Mao, H.-X. Ni and Y.-X. Zheng, *Adv. Funct. Mater.*, 2024, **34**, 2403803.
24 J. Jin, M. Chen, H. Jiang, B. Zhang, Z. Xie and W.-Y. Wong, *ACS Mater. Lett.*, 2024, **6**, 3246.
25 J. Jin, M. Chen, H. Jiang, B. Zhang, Z. Xie and W.-Y. Wong, *Adv. Opt. Mater.*, 2024, **12**, 2400794.
26 S. M. Pratik, V. Coropceanu and J.-L. Brédas, *ACS Mater. Lett.*, 2022, **4**, 440.
27 S. M. Pratik, E. P. McBride, J.-L. Brédas and V. Coropceanu, *Adv. Opt. Mater.*, 2025, **13**, 2403421.
28 S. Nathiya, M. Panneerselvam and L. T. Costa, *Phys. Chem. Chem. Phys.*, 2025, **27**, 7265.
29 J. Ochi, Y. Yamasaki, S. Oda, M. Kondo, A. Ikeno, Y. Kondo and T. Hatakeyama, *Adv. Opt. Mater.*, 2025, **13**, 2402939.
30 K. Matsui, S. Oda, K. Yoshiura, K. Nakajima, N. Yasuda and T. Hatakeyama, *J. Am. Chem. Soc.*, 2018, **140**, 1195.
31 S. Oda, B. Kawakami, Y. Yamasaki, R. Matsumoto, M. Yoshioka, D. Fukushima, S. Nakatsuka and T. Hatakeyama, *J. Am. Chem. Soc.*, 2022, **144**, 106.
32 Y. Sano, T. Shintani, M. Hayakawa, S. Oda, M. Kondo, T. Matsushita and T. Hatakeyama, *J. Am. Chem. Soc.*, 2023, **145**, 11504.
33 E. Cho, L. Liu, V. Coropceanu and J.-L. Brédas., *J. Chem. Phys.*, 2020, **153**, 144708.
34 (*a*) T. Lu and F. Chen, *J. Comput. Chem.*, 2012, **33**, 580; (*b*) T. Lu, *J. Chem. Phys.*, 2024, **161**, 082503.
35 M. Hagai, N. Inai, T. Yasuda, K. J. Fujimoto and T. Yanai, *Sci. Adv.*, 2024, **10**, eadk3219.
36 S. Oda, W. Kumano, T. Hama, R. Kawasumi, K. Yoshiura and T. Hatakeyama, *Angew. Chem., Int. Ed.*, 2021, **60**, 2882.
37 Y. Tanaka, T. Takahashi, J. Nishide, Y. Hiraga, H. Nakanotani and C. Adachi, *Thin Solid Films*, 2016, **619**, 120.
38 K. Togashi, S. Nomura, N. Yokoyama, T. Yasuda and C. Adachi, *J. Mater. Chem. C*, 2012, **22**, 20689.